PHOTONICS Research

Broadband mid-infrared supercontinuum generation in dispersion-engineered As_2S_3-silica nanospike waveguides pumped by 2.8 μm femtosecond laser

Pan Wang,[1] Jiapeng Huang,[1,4] Shangran Xie,[1,5] Johann Troles,[2] and Philip St.J. Russell[1,3]

[1]Max Planck Institute for the Science of Light, 91058 Erlangen, Germany
[2]Université de Rennes I, Sciences Chimiques de Rennes, 35042 Rennes, France
[3]Friedrich-Alexander-Universität, 91058 Erlangen, Germany
[4]e-mail: jiapeng.huang@mpl.mpg.de
[5]e-mail: shangran.xie@mpl.mpg.de

Received 18 November 2020; revised 10 February 2021; accepted 11 February 2021; posted 12 February 2021 (Doc. ID 415339); published 31 March 2021

Broadband mid-infrared (IR) supercontinuum laser sources are essential for spectroscopy in the molecular fingerprint region. Here, we report generation of octave-spanning and coherent mid-IR supercontinua in As_2S_3-silica nanospike hybrid waveguides pumped by a custom-built 2.8 μm femtosecond fiber laser. The waveguides are formed by pressure-assisted melt-filling of molten As_2S_3 into silica capillaries, allowing the dispersion and nonlinearity to be precisely tailored. Continuous coherent spectra spanning from 1.1 μm to 4.8 μm (30 dB level) are observed when the waveguide is designed so that 2.8 μm lies in the anomalous dispersion regime. Moreover, linearly tapered millimeter-scale As_2S_3-silica waveguides are fabricated and investigated for the first time, to the best of our knowledge, showing much broader supercontinua than uniform waveguides, with improved spectral coherence. The waveguides are demonstrated to be long-term stable and water-resistant due to the shielding of the As_2S_3 by the fused silica sheath. They offer an alternative route to generating broadband mid-IR supercontinua, with applications in frequency metrology and molecular spectroscopy, especially in humid and aqueous environments.

https://doi.org/10.1364/PRJ.415339

1. INTRODUCTION

Mid-infrared (IR) laser sources have received considerable attention over the past few decades due to important applications in molecular spectroscopy, biomedical science, materials processing, and remote sensing [1–4]. In particular, ultrabroadband and high-brightness mid-IR supercontinuum (SC) sources are of great interest since the fundamental vibrational resonances of many molecules reside in the mid-IR. Normally efficient generation of a mid-IR SC requires an ultrafast laser source coupled into a highly nonlinear waveguide. Several schemes have been implemented, based on, for example, optical parametric oscillators and amplifiers [5–7], Cr:ZnS/ZnSe mode-locked lasers [8,9], difference frequency generators [10], and rare-earth-doped fiber lasers [11–16]. Among them, fiber-based pump sources are preferable, owing to their high power-handling capabilities and the potential to be fully integrated as all-fiber SC sources [11–16]. The beam quality of fiber-based SC sources is also generally superior to that achieved in chip-based platforms [17–23]. Very recently, significant developments have been reported in femtosecond mid-IR fiber lasers at 2.8 μm. Such lasers now offer sub-megawatt-level peak powers and few-cycle pulse durations [24–27] and have great potential as pump sources for mid-IR SC generation.

Highly nonlinear fibers are normally made from compound "soft" glasses that are transparent at wavelengths above the 2.2 μm multi-phonon absorption band of fused silica [28]. Chalcogenide glasses are of particular interest, offering both transparency out to 25 μm [29,30] and ultra-high nonlinearities [31]. Even though many different chalcogenide fibers have been reported (examples being step-index fibers [5,8,12], photonic crystal fibers [9,15], and tapered fibers [7,16]), precise tuning of the waveguide dimensions and thus the dispersion and nonlinearity still remains challenging owing to difficulties in the thermal treatment of chalcogenide materials. In addition, many chalcogenides are mechanically fragile and suffer from glass degradation induced by humidity in the environment. Such drawbacks significantly limit the applications and long-term stability of chalcogenide-based devices.

A pressure-assisted melt-filling technique allowing chalcogenide glass to be integrated with fused silica capillaries has recently been reported [8,12,32–34]. It involves pumping molten chalcogenide glass into a silica capillary under high pressure. In the resulting structures, the chalcogenide is shielded from the environment by the fused silica sheath, greatly extending the device's mechanical stability and lifetime. The high index contrast between chalcogenide and silica glasses tightly confines mid-IR laser light within the core and ensures low-loss guidance. The ability to accurately engineer the geometry of the silica capillaries, using well-developed fiber fabrication and post-processing techniques, means that the dispersion and nonlinearity can be precisely controlled over a wide range. Nanospikes can be introduced at both ends of a subwavelength core, allowing efficient adiabatic launching of pump light into the fundamental waveguide mode and boosting the overall transmission [34].

Here, we report low-noise SC generation in As_2S_3-silica nanospike waveguides by extending the pump source to a recently developed 2.8 μm femtosecond fiber laser [27]. The nonlinear dynamics of SC generation in different specially designed dispersion regimes is investigated. A novel tapered As_2S_3-silica waveguide with a varying dispersion profile is fabricated and investigated for the first time, to the best of our knowledge, with broader SC and improved spectral coherence. Moreover, the long-term stability and water-resistance of the As_2S_3-silica hybrid waveguide are also experimentally demonstrated, revealing the potential of applications in humid and aqueous environments.

2. EXPERIMENTAL SETUP

The experimental setup is sketched in Fig. 1(A). The 2.8 μm wavelength (λ_0) fiber laser consists of a dispersion-managed seed laser and an amplifier [27]. The seed oscillator was a 3.3-m-long Er-doped ZBLAN fiber (gain fiber), backward pumped by a 975 nm laser diode, using folded Martinez stretchers for dispersion management. Mode-locking was by nonlinear polarization rotation. Pulses with duration 82 fs at a repetition rate of 42.1 MHz and a maximum average power of 1.2 W were generated after amplification in an Er-doped ZBLAN fiber. Figure 1(B) shows the measured auto-correlation trace of the output pulses at 1.2 W, showing a full width at half-maximum (FWHM) duration of 112 fs. The measured spectral intensity is plotted in Fig. 1(C), showing an FWHM bandwidth of ~200 nm.

Figure 1(D) is an optical micrograph of a fabricated As_2S_3-silica hybrid nanospike waveguide with core diameter $d = 5.4$ μm. A 250-μm-long nanospike was employed at the input end to allow adiabatic coupling of pump light into the fundamental HE_{11} core mode. The calculated (via finite element modeling) group velocity dispersion (GVD, top) and nonlinearity (bottom) of the HE_{11} mode are plotted in Fig. 1(E) for different core diameters. As the core diameter falls, the dispersion landscape evolves from showing a single zero-dispersion wavelength (ZDW), corresponding to the material dispersion of As_2S_3, to showing two ZDWs. The propagation loss of the waveguides [Fig. 1(F)] was estimated theoretically by taking into account the measured wavelength-dependent material loss of both As_2S_3 and fused silica, together with the modal overlap.

The pump light was coupled into the waveguide through an anti-reflection-coated black-diamond aspheric lens with a numerical aperture (NA) of ~0.85. A half-wave plate and a quarter-wave plate were used to adjust the polarization state of the input beam. The generated mid-IR SC spectra were collected by a commercial multimode InF_3 fiber connected to a Fourier transform IR spectrometer (FTIR).

3. EXPERIMENTAL RESULTS AND DISCUSSION

A. $d = 5.4$ μm Waveguide

As_2S_3-silica waveguides with constant core diameter were first investigated. Figure 2(A) shows the measured SC spectra

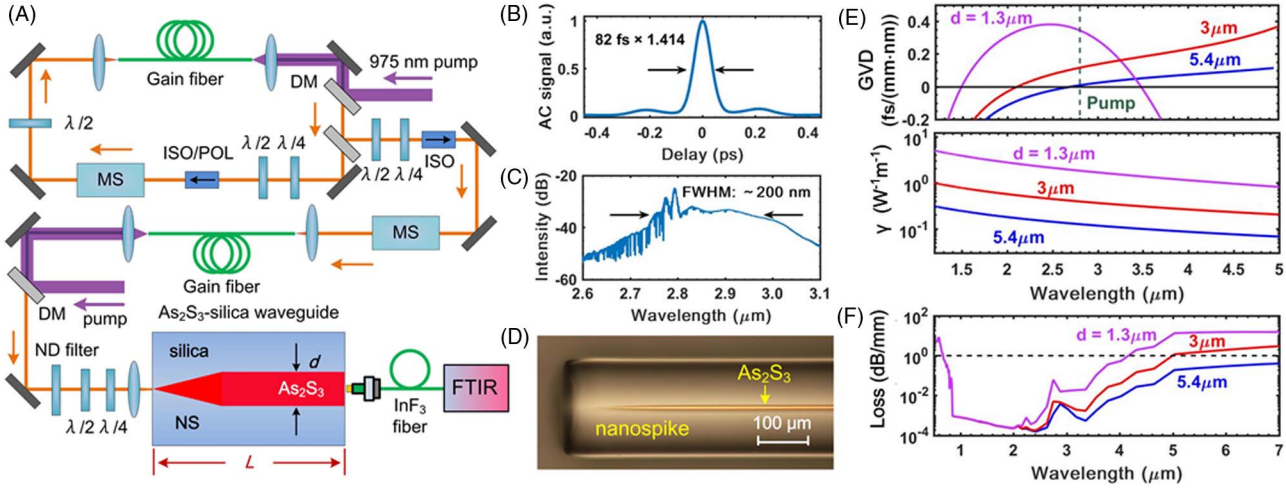

Fig. 1. (A) Experimental setup. DM, dichroic mirror; MS, Martinez stretcher; ISO, isolator; POL, polarizer; ND filter, neutral density filter; NS, nanospike; FTIR, Fourier transform IR spectrometer. (B) Measured auto-correlation trace and (C) the corresponding optical spectrum of the output pulses after the amplifier at an average power of 1.2 W. (D) Optical image of the As_2S_3-silica nanospike waveguide. The core diameter increases from 0 to 5.4 μm along the 250-μm-long taper transition region. (E) Simulated GVD (top), nonlinearity (bottom) and (F) propagation loss of the hybrid waveguides plotted against wavelength for different core diameters.

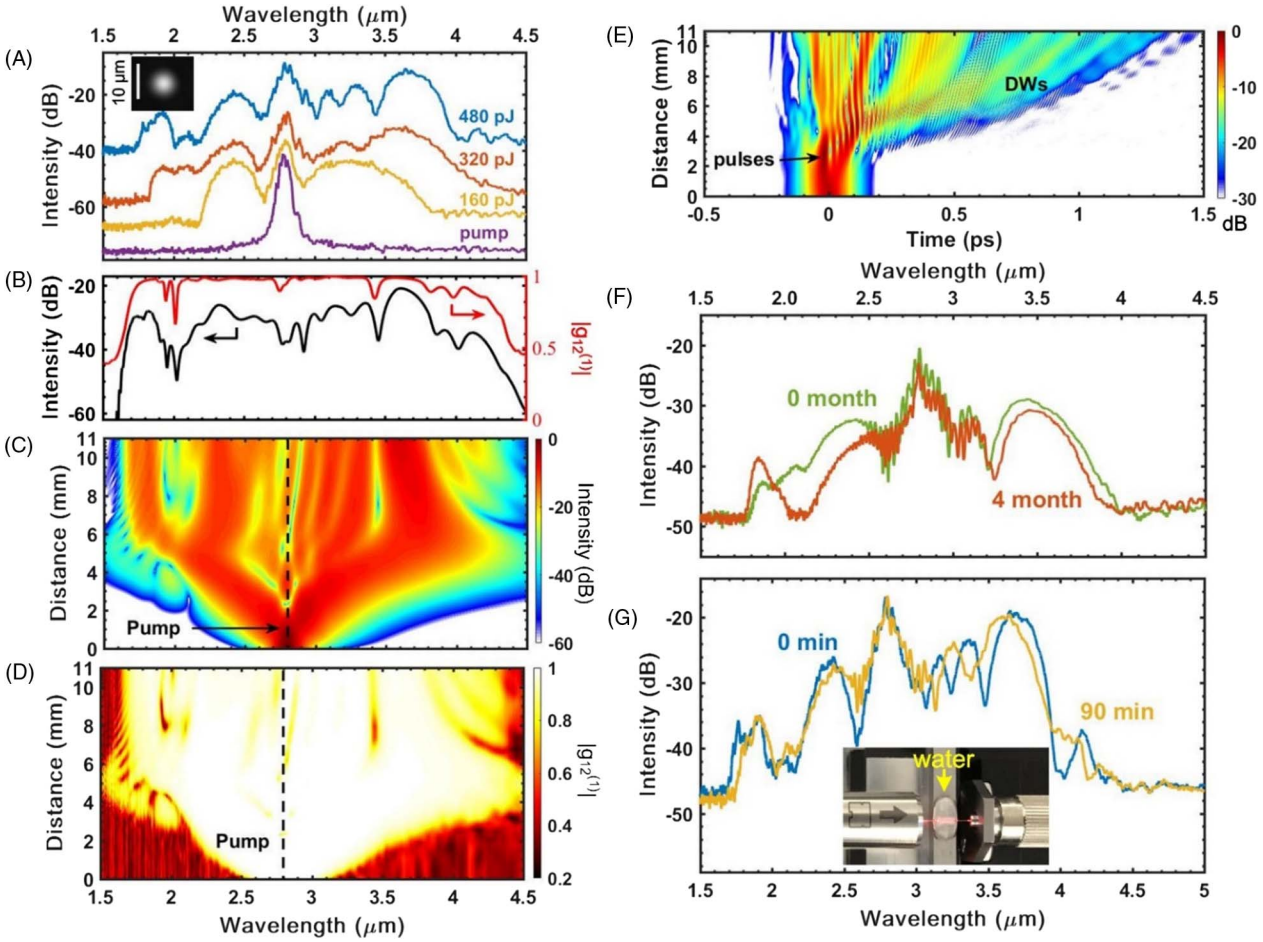

Fig. 2. (A) Measured SC spectra generated by the As_2S_3-silica waveguide with $d = 5.4$ μm under different coupled pump pulse energies. Inset: measured near-field mode image at the output end at 480 pJ coupled pulse energy. (B) Simulated SC spectrum (black) and its coherence (red) at the output face of the waveguide under a coupled pulse energy of 480 pJ. (C) Simulated SC spectral evolution along the 11-mm-long waveguide. (D) Simulated SC coherence evolution along the waveguide. (E) Simulated SC temporal evolution along the waveguide. (F) Long-term stability test of the waveguide under lab condition. (G) Water-resistant test of the hybrid waveguide. Inset: experimental setup.

generated in an 11-mm-long As_2S_3-silica waveguide with $d = 5.4$ μm for increasing pump pulse energy. In this situation, the 2.8 μm pump wavelength is located in the anomalous dispersion regime, close to the ZDW, as seen in the blue curve in Fig. 1(E) (top).

An octave-spanning SC (1.8 μm to 4.3 μm) was generated at a launched pulse energy of 320 pJ (the measured in-coupling efficiency was 4.2%). The dispersive wave (DW) emitted at ~1.8 μm was observed to blue shift with increasing pulse energy [35].

The SC spectrum was broadest at a maximum launched energy of 480 pJ (corresponding to 4.2 kW peak power), extending from 1.6 μm to 4.5 μm (30 dB level). At this pump energy, the average output power of the entire SC was more than 20 mW. Note that no damage in the nanospike waveguide was observed in the experiment after extended operation at the maximum pump power of 1.2 W.

The system was numerically simulated using the generalized nonlinear Schrödinger equation [36]:

$$\frac{\partial A(z,T)}{\partial z} = -\frac{\alpha}{2}A + i\sum_{k=2}^{\infty}\frac{i^k\beta_k}{k!}\frac{\partial^k}{\partial T^k}A + i\gamma\left(1 + i\tau_0\frac{\partial}{\partial T}\right)\left[A\int_{-\infty}^{\infty}R(\tau)|A(z,t-\tau)|^2\,\mathrm{d}\tau\right], \quad (1)$$

where $A(z, T)$ is the complex amplitude of the pulse envelope, z is the position, and T is the time in a reference frame traveling at the pulse group velocity. The first term on the right-hand side of Eq. (1) represents the optical loss determined by the linear loss coefficient α. β_k in the second term is the kth Taylor coefficient of the propagation constant $\beta(\omega)$, expanded about the central frequency $\omega_0 = 2\pi c/\lambda_0$.

The third term contains the Kerr nonlinearity (γ), stimulated Raman scattering, and the self-steepening effect. The normalized functional form $R(t) = (1 - f_R)\delta(t) + f_R h_R(t)$ includes both instantaneous electronic and delayed Raman contributions, where f_R denotes the fractional Raman

response. The analytical expression for the delayed Raman response is given by [33]

$$h_R(t) = (\tau_1^{-2} + \tau_2^{-2})\tau_1 \exp(-t/\tau_2)\sin(t/\tau_1), \quad (2)$$

where $f_R = 0.1$, $\tau_1 = 15.5$ fs, and $\tau_2 = 230.5$ fs for As_2S_3. The $i\tau_0\partial/\partial T$ term models the dispersion of the nonlinearity associated with the self-steepening effect, characterized by a time scale of $\tau_0 = 1/\omega_0$.

The simulated spectrum at the output face of the uniform $d = 5.4$ μm waveguide is plotted in Fig. 2(B) (black-solid) for a launched pulse energy of 480 pJ and agrees well with the measured spectrum. The corresponding spectral and temporal evolution along the 11-mm-long waveguide is depicted in Figs. 2(C) and 2(E), respectively. The input pulse, with soliton order $N \sim 10.6$ (similar to the value reported in previous work [34]), initially undergoes symmetric spectral broadening as a result of self-phase modulation (SPM), followed by soliton fission and DW emission after a propagation distance of ~5 mm. A DW is emitted at ~1.8 μm in the normal dispersion region, as predicted by the phase-matching condition [36,37]:

$$\Delta\beta_{DW} = \beta_{DW} - \beta(\omega_s) - \frac{\omega_{DW} - \omega_s}{v_g} - (1 - f_R)\gamma P = 0, \quad (3)$$

where ω_{DW} and ω_s are the angular frequencies of the DW and the driving soliton pulse (peak power P and group velocity v_g), and β_{DW} is the wavevector at the DW frequency.

The coherence of the SC spectrum was estimated numerically by adding one photon per mode of random quantum noise (with 1% intensity noise) to the pump pulses within the pump bandwidth and calculating the modulus of the complex degree of the first-order coherence [8,36]:

$$|g_{12}^{(1)}(\lambda)| = \left| \frac{\langle A_1^*(\lambda)A_2(\lambda)\rangle}{\sqrt{\langle|A_1(\lambda)|^2\rangle\langle|A_2(\lambda)|^2\rangle}} \right|, \quad (4)$$

where A_1 and A_2 are the complex field amplitudes of the generated SC pairs, and the angular brackets denote an ensemble average over independently generated SC pairs. In the simulations, 30 SC shots were used. The results are plotted as the solid red curve in Fig. 2(B), showing close-to-unity coherence over the entire spectral range. The corresponding coherence evolution along the waveguide is also shown in Fig. 2(D). It can be seen that a high spectral coherence is maintained in the initial SPM induced spectral broadening and the subsequent nonlinear process.

To assess the long-term stability of the hybrid waveguides, a sample was stored under ambient conditions (atmosphere pressure, 25°C, relative humidity ~33%) for four months. The SC spectra generated in fresh and stored samples were almost identical [Fig. 2(F)]; we attribute the slight difference mainly to incoupling variations. The water-resistance of the sample was tested by immersion in water [inset of Fig. 2(G)]. The generated SC barely changed over 90 min of immersion.

B. $d = 1.3$ μm Waveguide

Next, an As_2S_3-silica waveguide with $d = 1.3$ μm was tested. In this case [Fig. 1(E)], the pump wavelength lies between two ZDWs at 1.5 μm and 3.5 μm in the anomalous dispersion regime. The measured SC spectra with increasing launched pump energy are shown in Fig. 3(A). At pulse energy of

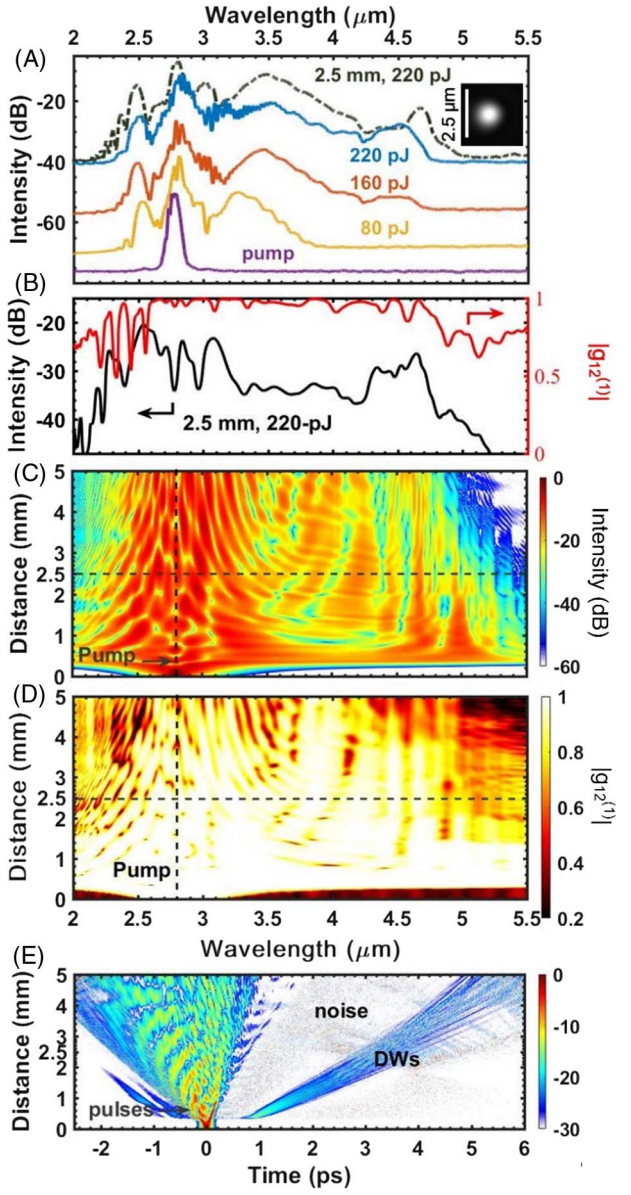

Fig. 3. (A) Measured SC spectra generated by the As_2S_3-silica waveguide with $d = 1.3$ μm at different launched pump pulse energies. Inset: measured output near-field mode image at 4.5 μm wavelength and 220 pJ coupled pulse energy. (B) Simulated output SC spectrum (black) and its coherence (red) for the cleaved 2.5-mm-long waveguide. (C) Simulated SC spectral evolution along the waveguide. (D) Simulated SC coherence evolution along the waveguide. (E) Simulated SC temporal evolution along the waveguide.

160 pJ, an octave-spanning SC extending from 2.2 μm to 4.7 μm was generated, with an emerging DW at 4.45 μm. Upon increasing the pump energy to 220 pJ, the DW band gets stronger and red shifts to 4.6 μm, and the SC spectrum broadens to 4.8 μm.

The measured near-field intensity profile of the light at 4.5 μm [inset of Fig. 3(A)] shows that it is in the fundamental mode. The total output power was measured as ~10 mW over the entire SC. Numerical simulations of SC evolution along the 5-mm-long waveguide [Fig. 3(C)] show that the input pulse

(soliton order ~4.4) experiences SPM induced spectral broadening followed by soliton fission and DW emission after propagation over less than 0.2 mm, due to the extremely high waveguide nonlinearity. The nonlinear dynamics of soliton fission as well as emission of the DWs can also be observed in the SC temporal evolution shown in Fig. 3(E).

Fundamental solitons emerge and are red shifted by the Raman effect, resulting in emission of several DW bands at shorter wavelengths, as predicted by phase-matching. It is worth noting that the DWs generated at longer wavelengths suffer attenuation due to material absorption. Bend loss is negligible here since the critical bend radius is estimated in the micrometer scale at the wavelength of 5 μm. As shown in Fig. 1(F), the propagation loss of the $d = 1.3$ μm waveguide is higher than 1 dB/mm at wavelengths above 4.2 μm due to the strong absorption of silica glass. The sample length was reduced to 2.5 mm by cleaving so as to decrease the total loss. The dark gray dotted curve in Fig. 3(A) plots the SC spectrum generated in the cleaved waveguide at the launched pulse energy of 220 pJ. An evident improvement in spectral broadening is observed, extending from 2.1 μm to 4.9 μm. The simulated output spectrum [black curve in Fig. 3(B)] at a distance of

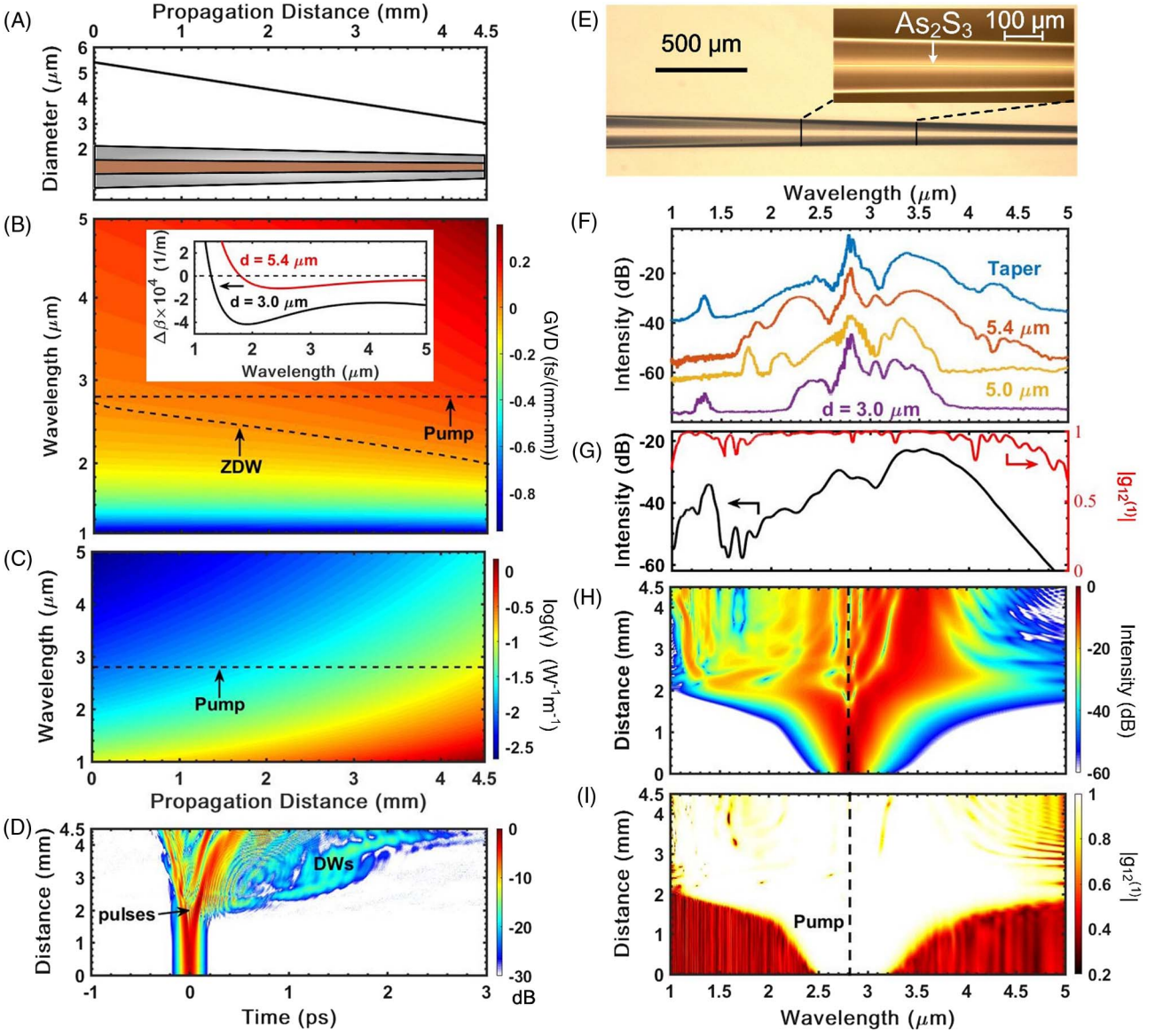

Fig. 4. (A) Core diameter of the dispersion-varying As_2S_3-silica waveguide plotted against distance. (B) Contour plot of the waveguide GVD versus wavelength and propagation distance for the waveguide in (A). Inset: calculated phase mismatch $\Delta\beta$ versus wavelength for $d = 5.4$ μm (red solid) and 3.0 μm (black solid). The dashed line marks the phase-matching condition ($\Delta\beta = 0$) for DW generation. (C) Contour plot of waveguide nonlinearity γ over propagation length for the waveguide in (A). (D) Simulated SC temporal evolution along the waveguide. (E) Optical image for one section of the fabricated tapered waveguide. (F) Measured SC spectra generated in the tapered waveguide shown in (A), compared with those generated in waveguides with constant core diameters. The launched pump energy was 490 pJ. (G) Simulated SC spectrum (black) and its coherence (red) for the tapered waveguide. (H) Simulated SC spectral evolution along the tapered waveguide. (I) Simulated SC coherence evolution along the tapered waveguide.

2.5 mm agrees well with the experimental results. The coherence evolution of the SC is displayed in Fig. 3(D). Significant spectral decoherence can be observed after a propagation of ~2 mm. We attribute this decoherence to the onset of strong random noise [Fig. 3(E)], due to the relatively high nonlinearity.

We also prepared a sample with a core diameter large enough that the pump wavelength lies in the normal dispersion regime. In this case, however, the nonlinearity is weaker, and the available pump pulse energy was not high enough to reach an octave-spanning SC.

C. Tapered Waveguide

Next, we explored SC generation in a tapered As_2S_3-silica waveguide. A silica capillary with inner diameter of 5.4 μm was first thermally tapered to 3.0 μm with a linear profile [Fig. 4(A)], and then filled with As_2S_3. The overall length of the tapered sample was ~4.5 mm. An optical image of the tapered waveguide is shown in Fig. 4(E), and its GVD and nonlinearity are plotted against wavelength and propagation distance in Figs. 4(B) and 4(C). The ZDW blue shifts from 2.7 μm to 2.1 μm along the down-tapered region, while the nonlinearity increases due to the decrease in modal area.

The measured SC spectra in the As_2S_3-silica waveguide with the constant core diameters and the tapered waveguide are shown in Fig. 4(F). The coupled pulse energy was 490 pJ. For the dispersion varying waveguide, two octave-spanning SC spectra can be obtained from 1.1 μm to 4.8 μm (30 dB level), which is broader than that in the fixed dispersion profiled waveguides. The calculated phase-matching condition for DW generation [$\Delta\beta$ from Eq. (3)] is plotted in the inset of Fig. 4(B) for waveguides with diameters of $d = 5.4$ μm and 3.0 μm.

The results show that the short-wavelength DW band blue shifts with decreasing core diameter and that the observed DW wavelength agrees well with theory. In the dispersion varying waveguide, DWs are continuously generated from 1.8 μm to shorter wavelengths as the soliton propagates along the taper, resulting in a broadening of the measured SC spectrum towards a shorter wavelength. The simulated SC temporal and spectral evolution along the tapered waveguide for a launched pulse energy of 490 pJ (soliton order $N \sim 10.5$) is plotted in Figs. 4(D) and 4(H). DW emission coincides with soliton fission at a propagation distance of ~1.2 mm. After the initial fission, the constituent solitons experience continuous shift to longer wavelengths due to the self-frequency shift. At the ~2.2 mm point, the DW dramatically blue shifts to a ~1.4 μm wavelength and results in a de-acceleration of the DW.

In addition, simulations indicate that the spectral coherence from a tapered waveguide is close to unity over the entire spectral range [red curve in Fig. 4(G)]—a significant improvement over fixed diameter waveguides [red curve in Figs. 2(B) and 3(B)]. Figure 4(I) plots the simulated spectral coherence evolution along the tapered waveguide, also showing an improved spectral coherence compared to Fig. 3(D). This might be explained by the suppression of noise-based modulation instability (MI) in the pulse in the tapered waveguides [38]. The MI gain spectrum is primarily determined by the GVD and nonlinearity. The fixed GVD and nonlinearity in constant diameter waveguides allow MI to build up strongly. In contrast, the continuously varying GVD and nonlinearity in a tapered waveguide strongly suppress the growth of MI. Temporal modulation of the pulse, seeded by random noise through MI, can therefore be effectively inhibited in a tapered structure, resulting in an improvement in spectral coherence. The temporal simulation in Fig. 4(D) validates the suppression of noises compared to Fig. 3(E).

4. CONCLUSIONS

Millimeter-scale chalcogenide-silica waveguides formed by pressure-assisted melt-filling provide an attractive alternative to waveguides formed on chip-scale platforms [17–23]. Further improvements in the filling technique will permit fabrication of more complex taper profiles optimized for SC generation [39]. The reported octave-spanning and coherent spectra could be directly used to realize a robust mid-IR frequency comb, since the output power level is adequate for $f-2f$ self-referencing interferometry, assuming stabilization of the repetition rate of the femtosecond pump laser. Despite having chalcogenide glass cores, the hybrid waveguides are uniquely water-resistant and long-term stable, properties that open up the possibility of applications in, e.g., biological spectroscopy in humid and aqueous environments. The SC spectral range could be further broadened into the IR using capillaries made from soft glasses such as germanates, fluorozirconates, or chalcogenides. The coupling efficiency of the waveguide may be further improved by polishing the in-coupling end after fabricating the nanospike structure. Profile-tunable As_2S_3-silica hybrid waveguides have great potential for applications in ultrafast nonlinear photonics, e.g., parametric processes in the mid-IR band.

Funding. Max-Planck-Gesellschaft.

Acknowledgment. We thank Dr. Francesco Tani for valuable suggestions on the theoretical modeling of the SC generation. S. X. and P. St.J. R. conceived the project. P. W. designed and fabricated the As_2S_3-silica hybrid waveguides. J. H. developed the ultrafast laser source. P. W. and J. H. carried out the SC generation experiments. J. T. provided the As_2S_3 material. All authors analyzed the data and wrote the paper.

Disclosures. The authors declare no conflicts of interest.

REFERENCES

1. R. R. Gattass and E. Mazur, "Femtosecond laser micromachining in transparent materials," Nat. Photonics **2**, 219–225 (2008).
2. A. B. Seddon, "A prospective for new mid-infrared medical endoscopy using chalcogenide glass," Int. J. Appl. Glass Sci. **2**, 177–191 (2011).
3. M. Kumar, M. N. Islam, F. L. Terry, M. J. Freeman, A. Chan, M. Neelakandan, and T. Manzur, "Stand-off detection of solid targets with diffuse reflection spectroscopy using a high-power mid-infrared supercontinuum source," Appl. Opt. **51**, 2794–2807 (2012).
4. S. Lambert-Girard, M. Allard, M. Piché, and F. Babin, "Differential optical absorption spectroscopy lidar for mid-infrared gaseous measurements," Appl. Opt. **54**, 1647–1656 (2015).
5. C. R. Petersen, U. Møller, I. Kubat, B. Zhou, S. Dupont, J. Ramsay, T. Benson, S. Sujecki, N. Abdel-Moneim, Z. Tang, D. Furniss, A. Seddon, and O. Bang, "Mid-infrared supercontinuum covering the

1.4–13.3 μm molecular fingerprint region using ultra-high NA chalcogenide step-index fibre," Nat. Photonics **8**, 830–834 (2014).
6. Z. Zhao, B. Wu, X. Wang, Z. Pan, Z. Liu, P. Zhang, X. Shen, Q. Nie, S. Dai, and R. Wang, "Mid-infrared supercontinuum covering 2.0–16 μm in a low-loss telluride single-mode fiber," Laser Photon. Rev. **11**, 1700005 (2017).
7. Y. Wang, S. Dai, G. Li, D. Xu, C. You, X. Han, P. Zhang, X. Wang, and P. Xu, "1.4–7.2 μm broadband supercontinuum generation in an As-S chalcogenide tapered fiber pumped in the normal dispersion regime," Opt. Lett. **42**, 3458–3461 (2017).
8. S. Xie, N. Tolstik, J. C. Travers, E. Sorokin, C. Caillaud, J. Troles, P. St.J. Russell, and I. T. Sorokina, "Coherent octave-spanning mid-infrared supercontinuum generated in As_2S_3-silica double-nanospike waveguide pumped by femtosecond Cr:ZnS laser," Opt. Express **24**, 12406–12413 (2016).
9. S. O. Leonov, Y. Wang, V. S. Shiryaev, G. E. Snopatin, B. S. Stepanov, V. G. Plotnichenko, E. Vicentini, A. Gambetta, N. Coluccelli, C. Svelto, P. Laporta, and G. Galzerano, "Coherent mid-infrared supercontinuum generation in tapered suspended-core $As_{39}Se_{61}$ fibers pumped by a few-optical-cycle Cr:ZnSe laser," Opt. Lett. **45**, 1346–1349 (2020).
10. I. Pupeza, D. Sánchez, J. Zhang, N. Lilienfein, M. Seidel, N. Karpowicz, T. Paasch-Colberg, I. Znakovskaya, M. Pescher, W. Schweinberger, V. Pervak, E. Fill, O. Pronin, Z. Wei, F. Krausz, A. Apolonski, and J. Biegert, "High-power sub-two-cycle mid-infrared pulses at 100 MHz repetition rate," Nat. Photonics **9**, 721–724 (2015).
11. H. Guo, C. Herkommer, A. Billat, D. Grassani, C. Zhang, M. H. P. Pfeiffer, W. Weng, C. Brès, and T. J. Kippenberg, "Mid-infrared frequency comb via coherent dispersive wave generation in silicon nitride nanophotonic waveguides," Nat. Photonics **12**, 330–335 (2018).
12. S. Xie, F. Tani, J. C. Travers, P. Uebel, C. Caillaud, J. Troles, M. A. Schmidt, and P. St.J. Russell, "As_2S_3-silica double-nanospike waveguide for mid-infrared supercontinuum generation," Opt. Lett. **39**, 5216–5219 (2014).
13. X. Jiang, N. Y. Joly, M. A. Finger, F. Babic, G. K. L. Wong, J. C. Travers, and P. St.J. Russell, "Deep-ultraviolet to mid-infrared supercontinuum generated in solid-core ZBLAN photonic crystal fibre," Nat. Photonics **9**, 133–139 (2015).
14. C. Yao, Z. Jia, Z. Li, S. Jia, Z. Zhao, L. Zhang, Y. Feng, G. Qin, Y. Ohishi, and W. Qin, "High-power mid-infrared supercontinuum laser source using fluorotellurite fiber," Optica **5**, 1264–1270 (2018).
15. S. Venck, F. St-Hilaire, L. Brilland, A. N. Ghosh, R. Chahal, C. Caillaud, M. Meneghetti, J. Troles, F. Joulain, S. Cozic, S. Poulain, G. Huss, M. Rochette, J. M. Dudley, and T. Sylvestre, "2–10 μm mid-infrared fiber-based supercontinuum laser source: experiment and simulation," Laser Photon. Rev. **14**, 2000011 (2020).
16. D. D. Hudson, S. Antipov, L. Li, I. Alamgir, T. Hu, M. E. Amraoui, Y. Messaddeq, M. Rochette, S. D. Jackson, and A. Fuerbach, "Toward all-fiber supercontinuum spanning the mid-infrared," Optica **4**, 1163–1166 (2017).
17. Y. Yu, X. Gai, P. Ma, D. Choi, Z. Yang, R. Wang, S. Debbarma, S. J. Madden, and B. Luther-Davies, "A broadband, quasi-continuous, mid-infrared supercontinuum generated in a chalcogenide glass waveguide," Laser Photon. Rev. **8**, 792–798 (2014).
18. N. Nader, A. Kowligy, J. Chiles, E. J. Stanton, H. Timmers, A. J. Lind, F. C. Cruz, D. M. B. Lesko, K. A. Briggman, S. W. Nam, S. A. Diddams, and R. P. Mirin, "Infrared frequency comb generation and spectroscopy with suspended silicon nanophotonic waveguides," Optica **6**, 1269–1276 (2019).
19. J. Yuan, Z. Kang, F. Li, X. Zhang, X. Sang, Q. Wu, B. Yan, K. Wang, X. Zhou, K. Zhong, G. Zhou, C. Yu, C. Lu, H. Y. Tam, and P. K. A. Wai, "Mid-infrared octave-spanning supercontinuum and frequency comb generation in a suspended germanium-membrane ridge waveguide," J. Lightwave Technol. **35**, 2994–3002 (2017).
20. M. Sinobad, C. Monat, B. Luther-Davies, P. Ma, S. Madden, D. J. Moss, A. Mitchell, D. Allioux, R. Orobtchouk, S. Boutami, J.-M. Hartmann, J.-M. Fedeli, and C. Grillet, "Mid-infrared octave-spanning supercontinuum and frequency comb generation in a suspended germanium-membrane ridge waveguide," Optica **5**, 360–366 (2018).
21. N. Singh, D. D. Hudson, Y. Yu, C. Grillet, S. D. Jackson, A. Casas-Bedoya, A. Read, P. Atanackovic, S. G. Duvall, S. Palomba, B. Luther-Davies, S. Madden, D. J. Moss, and B. J. Eggleton, "Midinfrared supercontinuum generation from 2 to 6 μm in a silicon nanowire," Optica **2**, 797–802 (2015).
22. J. Chiles, N. Nader, E. J. Stanton, D. Herman, G. Moody, J. Zhu, J. C. Skehan, B. Guha, A. Kowligy, J. T. Gopinath, K. Srinivasan, S. A. Diddams, I. Coddington, N. R. Newbury, J. M. Shainline, S. W. Nam, and R. P. Mirin, "Multifunctional integrated photonics in the mid-infrared with suspended AlGaAs on silicon," Optica **6**, 1246–1254 (2019).
23. M. Yu, B. Desiatov, Y. Okawachi, A. L. Gaeta, and M. Lončar, "Coherent two-octave-spanning supercontinuum generation in lithium-niobate waveguides," Opt. Lett. **44**, 1222–1225 (2019).
24. S. Duval, M. Bernier, V. Fortin, J. Genest, M. Piché, and R. Vallée, "Femtosecond fiber lasers reach the mid-infrared," Optica **2**, 623–626 (2015).
25. S. Antipov, D. D. Hudson, A. Fuerbach, and S. D. Jackson, "High-power mid-infrared femtosecond fiber laser in the water vapor transmission window," Optica **3**, 1373–1376 (2016).
26. C. Zhu, F. Wang, Y. Meng, X. Yuan, F. Xiu, H. Luo, Y. Wang, J. Li, X. Lv, L. He, Y. Xu, J. Liu, C. Zhang, Y. Shi, R. Zhang, and S. Zhu, "A robust and tuneable mid-infrared optical switch enabled by bulk Dirac fermions," Nat. Commun. **8**, 14111 (2017).
27. J. Huang, M. Pang, X. Jiang, F. Köttig, D. Schade, W. He, M. Butryn, and P. St.J. Russell, "Sub-two-cycle octave-spanning mid-infrared fiber laser," Optica **7**, 574–579 (2020).
28. S. D. Jackson, "Towards high-power mid-infrared emission from a fibre laser," Nat. Photonics **6**, 423–431 (2012).
29. B. J. Eggleton, B. Luther-Davies, and K. Richardson, "Chalcogenide photonics," Nat. Photonics **5**, 141–148 (2011).
30. V. S. Shiryaev and M. F. Churbanov, "Trends and prospects for development of chalcogenide fibers for mid-infrared transmission," J. Non-Cryst. Solids **377**, 225–230 (2013).
31. R. E. Slusher, G. Lenz, J. Hodelin, J. Sanghera, L. B. Shaw, and I. D. Aggarwal, "Large Raman gain and nonlinear phase shifts in high-purity As_2Se_3 chalcogenide fibers," J. Opt. Soc. Am. B **21**, 1146–1155 (2004).
32. M. A. Schmidt, L. Wondraczek, H. W. Lee, N. Granzow, N. Da, and P. St.J. Russell, "Complex Faraday rotation in microstructured magneto-optical fiber waveguides," Adv. Mater. **23**, 2681–2688 (2011).
33. N. Granzow, S. P. Stark, M. A. Schmidt, A. S. Tverjanovich, L. Wondraczek, and P. St.J. Russell, "Supercontinuum generation in chalcogenide-silica step-index fibers," Opt. Express **19**, 21003–21010 (2011).
34. N. Granzow, M. A. Schmidt, W. Chang, L. Wang, Q. Coulombier, J. Troles, P. Toupin, I. Hartl, K. F. Lee, M. E. Fermann, L. Wondraczek, and P. St.J. Russell, "Mid-infrared supercontinuum generation in As_2S_3-silica "nano-spike" step-index waveguide," Opt. Express **21**, 10969–10977 (2013).
35. W. Wang, H. Yang, P. Tang, C. Zhao, and J. Gao, "Soliton trapping of dispersive waves in photonic crystal fiber with two zero dispersive wavelengths," Opt. Express **21**, 11215–11226 (2013).
36. J. M. Dudley, G. Genty, and S. Coen, "Supercontinuum generation in photonic crystal fiber," Rev. Mod. Phys. **78**, 1135–1184 (2006).
37. B. Kuyken, M. Billet, F. Leo, K. Yvind, and M. Pu, "Octave-spanning coherent supercontinuum generation in an AlGaAs-on-insulator waveguide," Opt. Lett. **45**, 603–606 (2020).
38. N. Singh, D. Vermulen, A. Ruocco, N. Li, E. Ippen, F. X. Kärtner, and M. R. Watts, "Supercontinuum generation in varying dispersion and birefringent silicon waveguide," Opt. Express **27**, 31698–31712 (2019).
39. J. Wei, C. Ciret, M. Billet, F. Leo, B. Kuyken, and S. Gorza, "Supercontinuum generation assisted by wave trapping in dispersion-managed integrated silicon waveguides," Phys. Rev. Appl. **14**, 054045 (2020).